Computation of Green's functions for the acoustic scattering by an elastic structure excited by a turbulent flow in water

Louise Pacaut, Gilles Serre, Jean-François Mercier, Stéphanie Chaillat, Benjamin Cotté

25·29 August 2024
inter.noise
NANTES FRANCE

Computation of Green's functions for the acoustic scattering by an elastic structure excited by a turbulent flow in water

Louise Pacaut[1]
Gilles Serre[2]
Naval Group
199 Avenue Pierre-Gilles de Gennes, 83190 Ollioules, France

Jean-François Mercier[3]
Stéphanie Chaillat[4]
POEMS, ENSTA Paris, CNRS, INRIA, Institut Polytechnique de Paris
828 Boulevard des Maréchaux, 91120 Palaiseau, France

Benjamin Cotté[5]
IMSIA, ENSTA Paris, CNRS, CEA, EDF, Institut Polytechnique de Paris
828 Boulevard des Maréchaux, 91120 Palaiseau, France

ABSTRACT

To model the hydrodynamic noise produced by an elastic ship hull or propeller excited by a turbulent boundary layer, we need an efficient method to compute the acoustic scattering by an elastic body surrounded by a fluid. In 3D, Boundary Element Methods (BEM) are used to reduce the computational costs, for both the fluid and the elastic body. A natural way to compute the boundary integral representation (BIR) of the sound pressure is to use formulations based on the free space acoustic and elastic Green's functions. However, since the turbulent flow along the elastic body is known only statistically, the use of these Green's functions would be too expensive. A remedy is to compute a Green's function adapted to the physical problem, thus satisfying the transmission conditions of the fluid-structure problem. This so-called "tailored Green's function" is determined by solving a coupled acoustic-elastic problem with the BEM, and leads to a simplified BIR of the sound pressure compatible with a stochastic source term. We first validate the computation of the tailored Green's function over a classic spherical geometry. Then we compare the scattering of multiple quadrupoles by elastic or rigid NACA0012 profiles.

1. INTRODUCTION

When an immersed or partially-immersed structure moves in a fluid, a turbulent boundary layer appears around the structure. In underwater acoustics, because of the fluid loading, most structures

[1]louise.pacaut@ensta-paris.fr
[2]gilles.serre@naval-group.com
[3]jean-francois.mercier@ensta-paris.fr
[4]stephanie.chaillat@ensta-paris.fr
[5]benjamin.cotte@ensta-paris.fr

can not be considered as rigid and the elasticity of the structure has an effect on the acoustic scattering (see, for example, [1]). In the past few decades, various methods have developed to study the turbulent excitations over various types of obstacle. Many works introduce Green's functions that are called "tailored" to the considered obstacle, i.e that satisfy the transmission conditions of the fluid-structure problem. However, most of them are obtained analytically, and are therefore tailored to simple geometries such as steps [2] or hemisphere [3], or numerically over rigid geometries [4].
In this work, we propose to extend the concept of tailored Green's functions to an arbitrary geometry and to a complex coupling. In this aim, we develop a numerical method to determine a Green's function tailored to an elastic obstacle of arbitrary shape. We consider a coupled Boundary Element - Boundary Element Method (BEM-BEM). It is an alternative to coupled finite element methods (FEM-FEM or FEM-BEM) that require a mesh of the full 3D structure or CFD methods which are not very well suited for low Mach - high Reynolds underwater acoustic studies ([5], [6]).
The paper is divided as follows. First, we show the classical way to compute the boundary integral representation (BIR) of the sound pressure using the free space acoustic and elastic Green's functions. It is compared to the BIR using a tailored Green's function, and we show the interest of this last BIR when the source is a turbulent excitation. Then, we determine the system of coupled boundary integral equations leading to the numerical determination of the tailored Green's function. This numerical method is then validated over a classical simple sphere geometry. Finally, applications over an elastic NACA0012 profile in water are shown.

2. BEM/BEM FORMULATION FOR A FLUID-ELASTIC PROBLEM

The inner domain is noted Ω_s. It is an elastic solid of density ρ_s and of compressional and shear speeds c_p and c_s with the associated wavenumbers k_p and k_s. The exterior domain is noted Ω_f. It is a fluid of density ρ_f and speed c_f, associated to the wavenumber k_f. The coupled system is excited by a source S located in the exterior domain. The unknown in the interior problem is the total displacement noted $\mathbf{u}$. The unknown in the exterior problem is the total pressure noted p. Figure 1 gives a schematic representation of the coupling, recalling the notations.

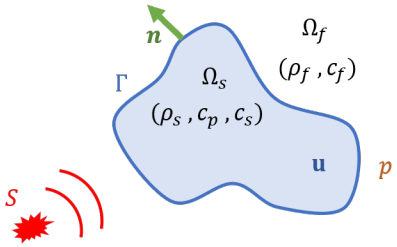

Figure 1: Schematic representation of the notations for a general fluid-structure coupling.

The total pressure in the exterior fluid domain is solution of the Helmholtz equation

$$(\Delta + k_f^2)p = -S \quad \text{in } \Omega_f, \tag{1}$$

and the total displacement is solution of the elastodynamic equation

$$\rho_s \omega^2 \mathbf{u} + \text{div}\sigma(\mathbf{u}) = 0 \quad \text{in } \Omega_s. \tag{2}$$

with $\sigma(\mathbf{u})$ the stress tensor. The 3 component vector unknown $\mathbf{u}$ and the scalar unknown p are connected by two boundary conditions at the interface:

– Continuity of the normal stresses:

$$\sigma(\mathbf{u})(\boldsymbol{x}).\mathbf{n}(\boldsymbol{x}) = \mathbf{t}(\boldsymbol{x}) = -p(\boldsymbol{x})\mathbf{n}(\boldsymbol{x}), \quad \forall \boldsymbol{x} \in \Gamma. \tag{3}$$

– Continuity of the normal displacements:

$$\left(\frac{\partial p}{\partial n}\right)(\boldsymbol{x}) = \rho_f \omega^2 \mathbf{u}(\boldsymbol{x}).\mathbf{n}(\boldsymbol{x}), \quad \forall \boldsymbol{x} \in \Gamma. \tag{4}$$

2.1. Boundary integral equations computed with the free field Green's function

A natural way to compute the total pressure and the total displacement in each domain Ω_f and Ω_s is to introduce the acoustic and elastic free field Green's functions [7] known in closed form. They lead to the following boundary integral representations.

Total pressure - Exterior problem. In the fluid domain, the integral representation of the solution of Equation 1 with the free field Green's function writes:

$$p(\boldsymbol{x}) = \int_{\Omega_f} S(\boldsymbol{y}) G_0(\boldsymbol{x}, \boldsymbol{y}) \mathrm{d}\boldsymbol{y} + \int_\Gamma \Big(p(\mathbf{Z}) \partial_{n_\mathbf{Z}} G_0(\boldsymbol{x}, \mathbf{Z}) - G_0(\boldsymbol{x}, \mathbf{Z}) \partial_{n_\mathbf{Z}} p(\mathbf{Z}) \Big) \mathrm{d}\Gamma_\mathbf{Z}, \tag{5}$$

where

$$G_0(\boldsymbol{x}, \boldsymbol{y}) = \frac{e^{ik_f|\boldsymbol{x}-\boldsymbol{y}|}}{4\pi|\boldsymbol{x}-\boldsymbol{y}|}. \tag{6}$$

Introducing the double and single layer potentials which, to any function $\phi(\mathbf{Z})$ defined for any $\mathbf{Z} \in \Gamma$, associate the functions:

$$(\mathcal{D}_f \phi)(\boldsymbol{x}) = \int_\Gamma \partial_{n_\mathbf{Z}} G_0(\boldsymbol{x}, \mathbf{Z}) \phi(\mathbf{Z}) \mathrm{d}\Gamma_\mathbf{Z} \quad \text{and} \quad (\mathcal{S}_f \phi)(\boldsymbol{x}) = \int_\Gamma G_0(\boldsymbol{x}, \mathbf{Z}) \phi(\mathbf{Z}) \mathrm{d}\Gamma_\mathbf{Z},$$

we obtain

$$p(\boldsymbol{x}) = P^{(0)}(\boldsymbol{x}) + (\mathcal{D}_f p)(\boldsymbol{x}) - \left(\mathcal{S}_f \frac{\partial p}{\partial n}\right)(\boldsymbol{x}), \tag{7}$$

where $P^{(0)} = \displaystyle\int_{\Omega_f} S(\boldsymbol{y}) G_0(\boldsymbol{x}, \boldsymbol{y}) \mathrm{d}\boldsymbol{y}$.

Total displacement - Interior problem. In the elastic domain, the fundamental solution (Green tensor) is given by [8]

$$\mathbf{U}_i^k(\boldsymbol{x}, \boldsymbol{y}) = \frac{1}{k_s^2 \mu} \left[\left(\delta_{qs}\delta_{ik} - \delta_{qk}\delta_{is} \right) \frac{\partial}{\partial x_q} \frac{\partial}{\partial y_s} G_s(\boldsymbol{x}, \boldsymbol{y}) + \frac{\partial}{\partial x_i} \frac{\partial}{\partial y_k} G_p(\boldsymbol{x}, \boldsymbol{y}) \right], \tag{8}$$

where

$$G_\alpha(\boldsymbol{x}, \boldsymbol{y}) = \frac{e^{ik_\alpha|\boldsymbol{x}-\boldsymbol{y}|}}{4\pi|\boldsymbol{x}-\boldsymbol{y}|}, \tag{9}$$

$\alpha = p$ or s, referring to the compressional or shear wavenumbers. Introducing $\mathbf{T}_i^k(\boldsymbol{x}, \boldsymbol{y}) = \sigma(\mathbf{U}_i^k)(\boldsymbol{x}, \boldsymbol{y}) \cdot \mathbf{n}$ defined by

$$\mathbf{T}_i^k(\boldsymbol{x}, \boldsymbol{y}) = \left[\lambda \delta_{ij}\delta_{kl} + \mu \left(\delta_{ih}\delta_{jl} + \delta_{jh}\delta_{il} \right) \right] \frac{\partial}{\partial y_l} \mathbf{U}_i^k(\boldsymbol{x}, \boldsymbol{y}) n_j(\boldsymbol{x}), \tag{10}$$

where λ and μ are the Lamé coefficients, the elastodynamic boundary integral equation is then, for $\boldsymbol{x} \in \Omega_s$ and $k = 1, 2$ and 3,

$$\mathbf{u}_k(\boldsymbol{x}) = \int_\Gamma \left[\mathbf{U}^k(\boldsymbol{x}, \mathbf{Z}) \cdot \mathbf{t}(\mathbf{Z}) - \mathbf{T}^k(\boldsymbol{x}, \mathbf{Z}) \cdot \mathbf{u}(\mathbf{Z}) \right] \mathrm{d}\Gamma_\mathbf{Z}. \tag{11}$$

To fit the previous notations, we introduce the layer potentials $\mathcal{D}_s$ and $\mathcal{S}_s$ defined by

$$(\mathcal{D}_s^k\phi)(\boldsymbol{x}) = \int_\Gamma \mathbf{T}^k(\boldsymbol{x},\mathbf{Z})\cdot\phi(\mathbf{Z})\,\mathrm{d}\Gamma_\mathbf{Z} \quad \text{and} \quad (\mathcal{S}_s^k\phi)(\boldsymbol{x}) = \int_\Gamma \mathbf{U}^k(\boldsymbol{x},\mathbf{Z})\cdot\phi(\mathbf{Z})\,\mathrm{d}\Gamma_\mathbf{Z}, \tag{12}$$

and Equation 11 then writes

$$\mathbf{u}_k(\boldsymbol{x}) = -(\mathcal{D}_s^k\mathbf{u})(\boldsymbol{x}) + (\mathcal{S}_s^k\mathbf{t})(\boldsymbol{x}). \tag{13}$$

System of boundary integral equations. As indicated by Equation 7 and Equation 13, to compute the total exterior pressure in Ω_f and the total displacement in Ω_s, their values must be first computed on Γ first. Using the traces on Γ of each operator, we deduce the coupled boundary integral equation system, verified on Γ

$$\begin{cases} \left(\dfrac{I}{2} - D_f\right)p + S_f\left(\dfrac{\partial p}{\partial n}\right) &= P^{(0)} \quad \text{on } \Gamma, \\ \left(\dfrac{\mathbf{u}_k}{2} + D_s^k\mathbf{u}\right) - S_s^k\mathbf{t} &= 0 \quad \text{on } \Gamma \quad \text{for } k=1,2,3, \end{cases} \tag{14}$$

where D_s and S_s are the trace of $\mathcal{D}_s$ and $\mathcal{S}_s$ and D_f and S_f those of $\mathcal{D}_f$ and $\mathcal{S}_f$. Using the boundary conditions Equation 3 and Equation 4, we can write the system verified by the total exterior pressure p and the total displacement $\mathbf{u}$

$$\begin{cases} \left(\dfrac{I}{2} - D_f\right)p + \rho_f\omega^2 S_f(\mathbf{u}.\mathbf{n}) &= P^{(0)} \quad \text{on } \Gamma, \\ \left(\dfrac{\mathbf{u}_k}{2} + D_s^k\mathbf{u}\right) + S_s^k(p\mathbf{n}) &= 0 \quad \text{on } \Gamma \quad \text{for } k=1,2,3. \end{cases} \tag{15}$$

The main drawback of Equation 15 is that when considering multiple sources S (leading to multiple $P^{(0)}$), this integral equation has to be solved again for each new source. Moreover, for turbulent sources $P^{(0)}$ is only known in a stochastic way, and the usual statistical solution is determined thanks to the ensemble average $< pp^* >$ of Equation 5. These two points lead to high computational costs when considering Equation 5. To avoid such unnecessary costly procedures, a useful alternative is to compute a tailored Green's function as presented in the next section.

2.2. Total pressure computed with the fluid-structure tailored Green's function

Let G be the Green's function defined in Ω_f tailored to the coupled problem, and $\mathbf{u}_G$ the associated total displacement in Ω_s. G and $\mathbf{u}_G$ are both solutions of Equation 1 to Equation 4 with $p \to G$, $\mathbf{u} \to \mathbf{u}_G$ and $S \to \delta$, leading to the following coupled problem:

$$\begin{cases} (\Delta + k_f^2)G &= -\delta \quad \text{in } \Omega_f \\ \rho_s\omega^2\mathbf{u}_G + \mathrm{div}\sigma(\mathbf{u}_G) &= 0 \quad \text{in } \Omega_s \\ \sigma(\mathbf{u}_G).\mathbf{n} &= -G\boldsymbol{n} \quad \text{on } \Gamma \\ \dfrac{\partial G}{\partial n} &= \rho_f\omega^2\mathbf{u}_G.\boldsymbol{n} \quad \text{on } \Gamma \end{cases} \tag{16}$$

Equation 5 holds for any Green's function and we can write for $\boldsymbol{x} \in \Omega_f$

$$p(\boldsymbol{x}) = \int_{\Omega_f} S(\boldsymbol{y})G(\boldsymbol{x},\boldsymbol{y})\mathrm{d}\boldsymbol{y} + \int_\Gamma p(\mathbf{Z})\frac{\partial G(\boldsymbol{x},\mathbf{Z})}{\partial n_\mathbf{Z}} - G(\boldsymbol{x},\mathbf{Z})\frac{\partial p(\mathbf{Z})}{\partial n_\mathbf{Z}}\mathrm{d}\Gamma_\mathbf{Z}. \tag{17}$$

However, the main interest of the choice of G is that it leads to a surface integral equal to 0. To see this, we first recall that in Ω_s:

$$\begin{cases} \rho_s\omega^2\mathbf{u} + \mathrm{div}\sigma(\mathbf{u}) &= 0, \\ \rho_s\omega^2\mathbf{u}_G + \mathrm{div}\sigma(\mathbf{u}_G) &= 0. \end{cases} \tag{18}$$

Multiplying the first line by $\mathbf{u}_G$ and the second line by $\mathbf{u}$, then integrating over Ω_s, we get

$$\int_{\Omega_s} \mathrm{div}\sigma(\mathbf{u}_G)\mathbf{u} - \mathrm{div}\sigma(\mathbf{u})\mathbf{u}_G = 0. \tag{19}$$

After an integration by parts and noting that $\sigma(\mathbf{u}_G)\mathbf{u} = \sigma(\mathbf{u})\mathbf{u}_G$ because of the symmetry properties of the elastic constitutive equation, we get the reciprocity relation

$$\int_{\Gamma} -(\sigma(\mathbf{u}).\mathbf{n})(\mathbf{u}_G.\mathbf{n}) + (\sigma(\mathbf{u}_G).\mathbf{n})(\mathbf{u}.\mathbf{n}) = 0. \tag{20}$$

Finally, using the boundary conditions in Equation 3, Equation 4 and Equation 16 gives

$$\int_{\Gamma} p\frac{\partial G}{\partial n} - G\frac{\partial p}{\partial n} = 0. \tag{21}$$

Therefore, the tailored Green's function G leads to

$$p(\boldsymbol{x}) = \int_{\Omega_f} S(\boldsymbol{y})G(\boldsymbol{x},\boldsymbol{y})\mathrm{d}\boldsymbol{y}. \tag{22}$$

The main advantage of Equation 22 against Equation 5 is obvious: we no longer need to invert a boundary integral equation system when the source is changed. Once G is determined, we can directly compute p for any source S. This formulation is therefore more convenient for statistical studies linked to turbulence. Now that we have defined such a tailored Green's function, we show how to compute it.

3. DEFINITION AND COMPUTATION OF THE TAILORED GREEN'S FUNCTION

The goal is to write G and $\mathbf{u}_G$ versus the acoustic and elastic free field Green's functions, which are known analytically. Since $\mathbf{u}_G$ is a solution of Equation 2, we use Equation 11 with $\mathbf{u} \to \mathbf{u}_G$, which can be written $\forall \boldsymbol{x} \in \Omega_s$

$$(\mathbf{u}_G)_k(\boldsymbol{x}) = \int_{\Gamma} U^k(\boldsymbol{x},\mathbf{Z}) \cdot [\sigma(\mathbf{u}_G)(\mathbf{Z}).\mathbf{n}(\mathbf{Z})] - T^k(\boldsymbol{x},\mathbf{Z}) \cdot u_G(\mathbf{Z})\mathrm{d}\Gamma_{\mathbf{Z}}. \tag{23}$$

In the same way, since G is solution of the Helmholtz Equation 16, we use Equation 5 with $S \to \delta$ and $p \to G$, which can be written $\forall(\boldsymbol{x},\boldsymbol{y}) \in \Omega_f \times \Omega_f$

$$G(\boldsymbol{x},\boldsymbol{y}) = G_0(\boldsymbol{x},\boldsymbol{y}) + \int_{\Gamma} G(\boldsymbol{x},\mathbf{Z})\frac{\partial G_0(\boldsymbol{y},\mathbf{Z})}{\partial n_{\mathbf{Z}}} - G_0(\boldsymbol{y},\mathbf{Z})\frac{\partial G(\boldsymbol{x},\mathbf{Z})}{\partial n_{\mathbf{Z}}}\mathrm{d}\Gamma_{\mathbf{Z}}. \tag{24}$$

We can therefore write a system close to Equation 15, verified by G and $\mathbf{u}_G$ on the boundary Γ:

$$\begin{cases} \left(\dfrac{I}{2} - D_f\right)G + \rho_f\omega^2 S_f(\mathbf{u}_G.\mathbf{n}) &= G_0 \quad \text{on } \Gamma, \\ \left(\dfrac{(\mathbf{u}_G)_k}{2} + D_s^k\mathbf{u}_G\right) + S_s^k(G\mathbf{n}) &= 0 \quad \text{on } \Gamma \end{cases}. \tag{25}$$

We see that the computation of the tailored Green's function G does not depend on the source. It depends on G_0, the geometry and the physical characteristics of the media. Therefore, for a fixed geometry and fixed coupling parameters, the computation of G remains the same for any source. This, again, lays the emphasis on the benefits of using G instead of G_0 when an obstacle is excited by a turbulent flow. A direct resolution of Equation 25 can lead to numerical issues. Indeed, going back to Equation 25, each term of the system is of rough estimate orders

$$\begin{pmatrix} \mathrm{O}(1) & \mathrm{O}\left(\rho_f\omega^2\right) \\ \mathrm{O}\left(\frac{1}{k_s}\right) & \mathrm{O}\left(\frac{1}{\rho_s\omega^2}\right) \end{pmatrix}, \tag{26}$$

which, at 100 Hz and for aluminum bronze in water gives

$$\begin{pmatrix} \mathrm{O}(1) & \mathrm{O}\left(10^{9}\right) \\ \mathrm{O}\left(10^{-1}\right) & \mathrm{O}\left(10^{-10}\right) \end{pmatrix}. \tag{27}$$

Thus, the second line of the matrix is much smaller than the first and Equation 25 revealed to be ill-conditioned. A direct resolution of the system does not give an accurate result. A remedy, presented in [9], is to introduce a change of unknowns such that

$$\mathbf{u}_G^s = \rho_f\omega^2\mathbf{u}_G,$$

which leads to the system

$$\begin{cases} \left(\frac{I}{2} - D_f\right)G & + & S_f\left(\mathbf{u}_G^s.\mathbf{n}\right) & = & G_0 \quad \text{on } \Gamma, \\ \left(\frac{(\mathbf{u}_G^s)_k}{2} + D_s^k\mathbf{u}_G^s\right) & + & \rho_f\omega^2 S_s^k(G\mathbf{n}) & = & 0 \quad \text{on } \Gamma. \end{cases} \tag{28}$$

This leads to the new rough estimates

$$\begin{pmatrix} \mathrm{O}(1) & \mathrm{O}(1) \\ \mathrm{O}\left(\frac{1}{k_s}\right) & \mathrm{O}\left(\frac{\rho_f}{\rho_s}\right) \end{pmatrix} \approx \begin{pmatrix} \mathrm{O}(1) & \mathrm{O}(1) \\ \mathrm{O}\left(10^{-1}\right) & \mathrm{O}\left(10^{-1}\right) \end{pmatrix}. \tag{29}$$

Then, Equation 28 is well-conditioned and is used to compute $(G, \mathbf{u}_G)$ on the boundary Γ. The computation of the tailored Green's function in the fluid thanks to Equation 24 takes two steps. The first is to determine G and $\mathbf{u}_G$ on the boundary of the elastic structure, with Equation 28. The second step is then to compute G in all the fluid volume Ω_f thanks to Equation 24. In the next section, we present numerical validations of Equation 28 and of Equation 24.

4. NUMERICAL VALIDATION OF THE COMPUTATION OF G OVER AN ELASTIC SPHERE

Analytical solution of the tailored Green's function. In order to validate our numerical implementation to solve Equation 28 and Equation 24, we need a reference solution. Such a reference solution exists in the simple case of a spherical obstacle. For Ω_s a sphere of radius a, the tailored Green's function for the coupled fluid-structure problem can be explicitly determined, adapting [10], thanks to a modal expansion on the spherical Bessel functions basis:

$$G_0(\boldsymbol{x}, \boldsymbol{y}) = \frac{ik_f}{4\pi}\sum_{n=0}^{\infty}(2n+1)f_n \begin{cases} j_n(k_f r_x)h_n(k_f r_y) & r_y > r_x, \\ j_n(k_f r_y)h_n(k_f r_x) & a < r_y < r_x, \end{cases} \tag{30}$$

with f_n defined, for $\boldsymbol{x} = (r_x, \theta_x, \phi_x)$ and the same for $\boldsymbol{y}$, by

$$f_n(\theta_x, \theta_y, \varphi_x, \varphi_y) = \sum_{m=0}^{\infty}(2-\delta_{m0})\frac{(n-m)!}{(n+m)!}\cos\left[m(\varphi_x - \varphi_y)\right]P_n^m(\cos\theta_x)P_n^m(\cos\theta_y). \tag{31}$$

In presence of an elastic sphere, the Green's function becomes $G = G_0 + G^s$ with the scattered field G^s of the form

$$G^s(\boldsymbol{x},\boldsymbol{y}) = \frac{ik_f}{4\pi}\sum_{n=0}^{\infty}(2n+1)c_n f_n h_n(k_f r_x)h_n(k_f r_y). \tag{32}$$

Only c_n remains to be determined, which is done thanks to the boundary conditions given in Equation 16. In [11], ways to determine c_n are given for a spherical elastic obstacle in the case of a plane wave excitation. The determination of c_n remains the same here, only the plane wave excitation is replaced by G_0. Note that we are only interested in G but $\mathbf{u}_G$ can also be determined analytically.

Numerical validation over elementary cases. To validate the numerical procedure, we use the code COFFEE developed at POEMS[6]. We consider a sphere of radius $a = 1\,m$ associated to a mesh with 2 886 nodes and 5 768 elements. It is filled with plastic of density $\rho = 1\,800\,kg.m^{-3}$, compressional sound speed $c_p = 2\,400\,m.s^{-1}$ and shear sound speed $c_s = 1\,560\,m.s^{-1}$. The source $\boldsymbol{y}$ is placed at $(0, 0, 2\,m)$, the observer $\boldsymbol{x}$ at $(0, 0, 10\,m)$ and the frequency varies from 20 to 700 Hz. Results on figure 2 show a perfect agreement between analytical and numerical computations.

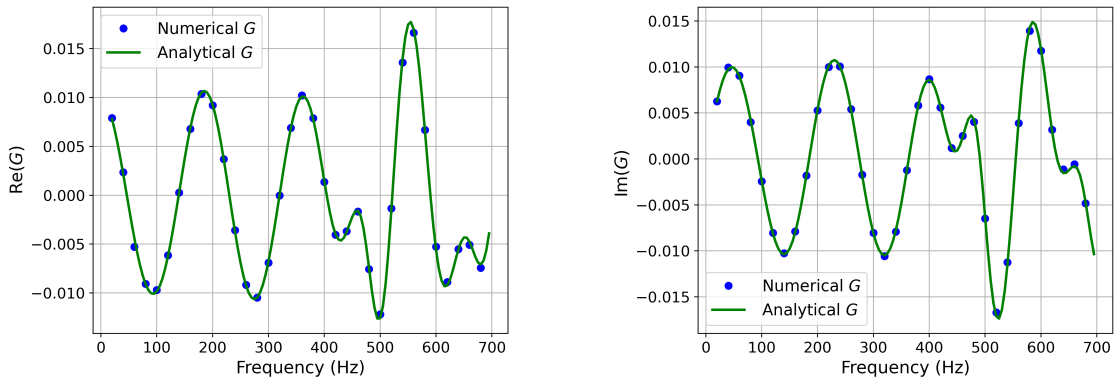

(a) Real part

(b) Imaginary part

Figure 2: Comparison between numerical and analytical Green's function tailored to an elastic sphere. The sphere is of radius $a = 1\,m$ and filled with plastic such that $\rho_s = 1\,800 kg/m^3$, $c_p = 2\,400 m/s$, $c_s = 1\,560 m/s$. The source $\boldsymbol{y}$ is placed at $(0, 0, 2\,m)$ and the observer $\boldsymbol{x}$ at $(0, 0, 10\,m)$.

5. APPLICATION TO A NACA0012 PROFILE IN WATER

We consider now a more complex geometry consisting of a NACA0012 profile of aluminium bronze ($\rho = 7\,640\,kg.m^{-3}$, $c_p = 4\,400\,m.s^{-1}$, $c_s = 2\,350\,m.s^{-1}$), of chord $c = 0.2\,m$ and width $L = 0.45\,m$, embedded in water. In the following, the profile is associated to a mesh of 2 582 nodes and 5 160 elements. We want to model the industrial configuration of a profile excited by a turbulent boundary layer. The Lighthill equation models the turbulence as a continuous distribution of quadrupoles [12], and we choose the simplified configuration of a discrete distribution of quadrupole sources. For one quadrupole, it corresponds to take $S = \partial y_i \partial y_j \delta(\boldsymbol{x} - \boldsymbol{y})$ and thus to take an incident pressure of the form

$$\Psi^{inc}(\boldsymbol{x},\boldsymbol{y}) = \frac{\partial^2 G_0(\boldsymbol{x},\boldsymbol{y})}{\partial y_1 \partial y_2}, \tag{33}$$

where y_k is k^{th} coordinate of $\boldsymbol{y}$. We consider here a lateral quadrupole but the study can be extended to a longitudinal quadrupole. The total field resulting from excitation Ψ^{inc} is

$$\Psi(\boldsymbol{x},\boldsymbol{y}) = \frac{\partial^2 G(\boldsymbol{x},\boldsymbol{y})}{\partial y_1 \partial y_2}. \tag{34}$$

[6]https://uma.ensta-paris.fr/soft/COFFEE/

Since $G_s = G - G_0$ is the scattered field generated by G_0, the scattered field resulting from excitation Ψ^{inc} is

$$\Psi_s(\boldsymbol{x}, \boldsymbol{y}) = \frac{\partial^2 G_s(\boldsymbol{x}, \boldsymbol{y})}{\partial y_1 \partial y_2}. \tag{35}$$

We suggest to focus on two configurations: (i) a trailing edge and (ii) a leading edge excited by one or multiple quadrupole sources. In each configuration, we first focus on the influence of the distance of the source on the resulting field. Then, we compare the field scattered by an elastic profile to a rigid profile.

Trailing edge noise. First, we consider quadrupole sources located downstream of the trailing edge and we study the influence of the distance of the source on the resulting field. The observer $\boldsymbol{x}$ rotates around $\mathbf{e}_3$, at a radius $R_x = 100\,m$ and we consider three different source positions (see fig. 3). The frequency is set such that $k_1 = 0.1\,m^{-1}$ (such that $k_1 c = 0.02 << 1$). Fig. 4 shows the comparison of the directivity diagrams for the three different source positions exciting an elastic aluminium bronze profile. We see that the closer the source is, the larger the magnitude of the scattered field is and thus quadrupole sources are more active when close to the obstacle surface. This confirms that the scattering due to turbulent boundary layers must not be ignored ([13], [14]). Moreover, we see that as the source moves away from the edge, the free field becomes dominant and therefore the total field recovers its quadrupolar directivity.

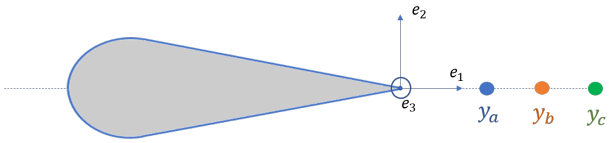

Figure 3: Quadrupole sources behind the trailing edge: $\boldsymbol{y}_a = (0.3c, 0, 0)$, $\boldsymbol{y}_b = (1.8c, 0, 0)$ and $\boldsymbol{y}_c = (4.3c, 0, 0)$, with $c = 0.2\,m$. The dimensions are note scaled on the figure.

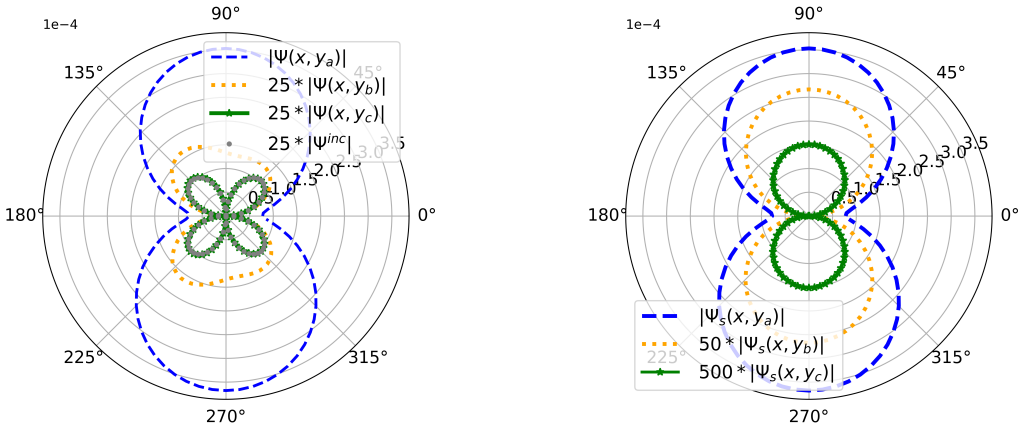

(a) Total Field

(b) Scattered field

Figure 4: Comparison between the total and scattered fields obtained for three different positions of the source $\boldsymbol{y}$. The sources are placed such as in fig. 3, the observer rotates around $\mathbf{e}_3$ at $R_x = 100\,m$ and the frequency is set such that $k_1 = 0.1\,m^{-1}$ ($k_1 c = 0.02$). To help results visualization, the amplitude of the scattered field obtained for sources at $\boldsymbol{y}_b$ and $\boldsymbol{y}_c$ are multiplied by 25, 50 or 500. The free field $|\Psi^{inc}|$, plotted on the total field directivity diagram, is obtained when there is no profile.

Next, we look at the influence of elasticity on the scattered field. The source is located behind the trailing edge at $\boldsymbol{y}_a = (0.3c, 0, 0)$. To simplify the results interpretation, the frequency is higher than previously and set such that $k_1 = 4.2\,m^{-1}$ (such that $k_1 c = 0.84 \approx 1$). The observer rotates again

around $\mathbf{e}_3$, with a radius $R_x = 100\,m$. Figure 5 shows a comparison between the directivity diagrams obtained for an elastic profile of aluminium bronze and for a rigid profile. We see that an elastic edge reduces the scattered field resulting from a quadrupole excitation, as expected in [1].

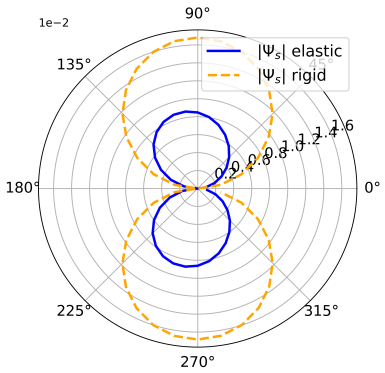

Figure 5: Comparison between the scattered field obtained with an elastic (filled line) and rigid (dashed line) profile. The source is placed downstream of the trailing edge at $\boldsymbol{y}_a = (0.3c, 0, 0)$, the observer rotates around $\mathbf{e}_3$ at $R_x = 100\,m$ and the frequency is set such that $k_1 = 4.2\,m^{-1}$ ($k_1 c = 0.8$).

Leading edge noise. As previously, we first study the influence of the distance of the source on the resulting field. A source is placed at three locations upstream of the leading edge (see fig. 6). The observer rotates around $\mathbf{e}_3$ at $R_x = 100\,m$ and the frequency is set such that $k_1 = 0.1\,m^{-1}$ ($k_1 c = 0.02$). Fig. 7 shows the comparison of the directivity diagrams for the three different sources. The same comments can be made as previously. In particular the closer to the surface the quadrupole source is, the larger the magnitude of the resulting fields. The difference of amplitude between Fig. 7 and Fig. 4 (almost 2 times higher for the leading edge than for the trailing edge) is due to the geometry of the edge [15].

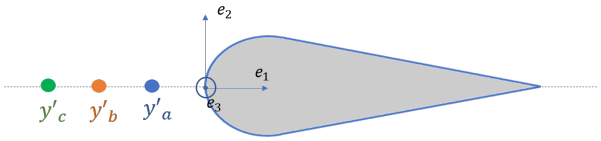

Figure 6: Quadrupole sources behind the leading edge: $\boldsymbol{y}'_a = (-0.3c, 0, 0)$, $\boldsymbol{y}'_b = (-1.8c, 0, 0)$ and $\boldsymbol{y}'_c = (-4.3c, 0, 0)$, with $c = 0.2\,m$.

Our goal is now to show the capacity of our method to take into account a more complicated type of source. The leading edge of the profile is excited by a volume of turbulence defined such as in figure 8. We consider a simplified deterministic turbulence description made of quadrupole sources randomly placed in the turbulence volume, easier to consider than the deterministic forcing models under study in the past ([16], [17]). We consider N=10 quadrupole sources and the total field resulting from the multiple quadrupole excitation is

$$\Psi = \sum_{j=1}^{N} \frac{\partial^2 G(\boldsymbol{x}, \boldsymbol{y}^j)}{\partial y_1^j \partial y_2^j} e^{-i\phi_j}, \tag{36}$$

with ϕ_j random phase angles applied to source at $\boldsymbol{y}^j$, in order to consider incoherent excitations. In the same way, the scattered field is

$$\Psi_s = \sum_{j=1}^{N} \frac{\partial^2 G_s(\boldsymbol{x}, \boldsymbol{y}^j)}{\partial y_1^j \partial y_2^j} e^{-i\phi_j}. \tag{37}$$

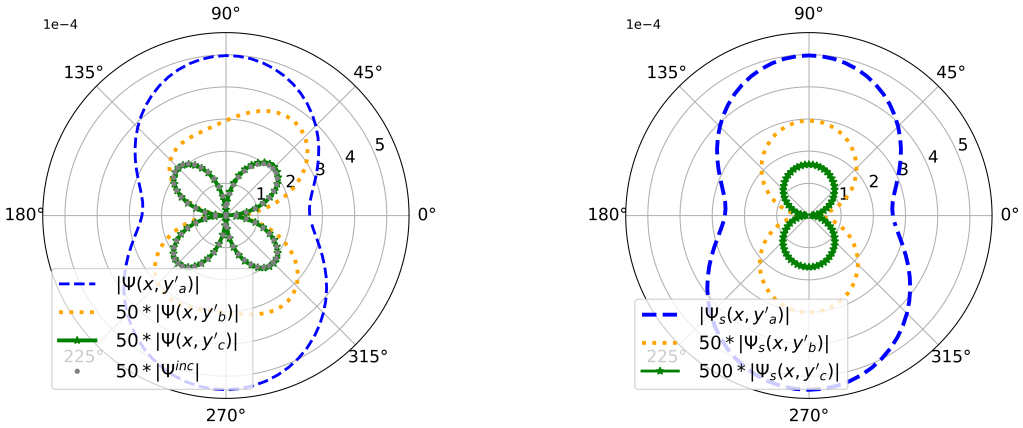

(a) Total Field (b) Scattered field

Figure 7: Comparison between the total and scattered fields obtained for three different positions of the source $\boldsymbol{y}$ at the leading edge. The sources are placed such as in fig. 6, the observer rotates around $\mathbf{e}_3$ at $R_x = 100\,m$ and the frequency is set such that $k_1 = 0.1\,m^{-1}$ ($k_1 c = 0.02$). For visibility issues, the amplitude of the scattered field obtained for sources at $\boldsymbol{y}_b$ and $\boldsymbol{y}_c$ are multiplied by 50 or 500. The free field is plotted on the total field directivity diagram.

With this configuration, we see the interest of computing a tailored Green's function: only one computation of the boundary integral equation system (Equation 28) is needed for all the 10 sources. Then, 10 boundary integral representations (Equation 24) are computed, but computing Equation 24 is much less expensive than solving Equation 28.

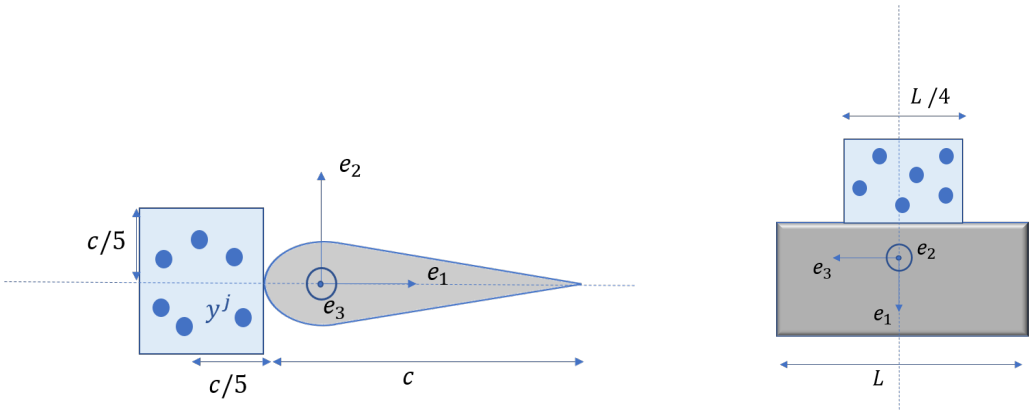

(a) View from the side (b) View from above

Figure 8: Schematic representation of the turbulence volume, modeled by a finite number N of quadrupole sources, located at $\boldsymbol{y}^j$, $j = 1,\ldots,N$. c=0.2 m and L=0.45 m. The dimensions are not scaled on the figure.

Figure 9 shows a comparison between the scattered field Ψ_s obtained when the profile is elastic (aluminium bronze) and when it is rigid. The observer rotates around $\mathbf{e}_3$ at $R_x = 100\,m$ and the frequency is set such that $k_1 = 4.2\,m^{-1}$ (such that $k_1 c = 0.84$). As for one source, we see that the leading edge noise due to multiple quadrupole excitation is reduced when the profile is elastic compared to when it is rigid. This is in agreement with the results for trailing edge noise.

6. CONCLUSION AND PERSPECTIVE

We propose a BEM-BEM coupling method to determine a Green's function tailored to an elastic structure embedded in a fluid. We have shown that the computation of the tailored Green's function

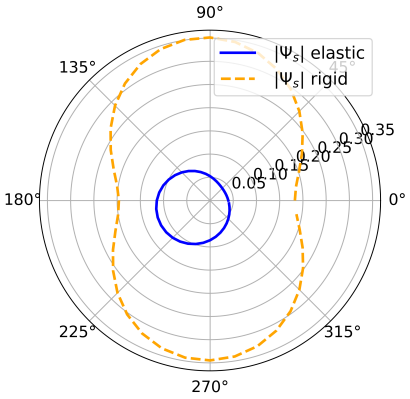

Figure 9: Comparison between the scattered field -Equation 37 - of an elastic profile (filled line) and a rigid profile (dashed line) excited by N=10 quadrupole sources randomly placed in the turbulence volume described in fig. 8. The observer rotates around $\mathbf{e}_3$ at $R_x = 100\,m$ and the frequency is set such that $k_1 = 4.2\,m^{-1}$ (such that $k_1 c = 0.84$).

does not depend on the source type and its use is therefore well suited to the study of a stochastic turbulent excitation. The computation of the tailored Green's function is validated over the simple geometry case of a sphere. Then, to show the capability of the method, applications over an elastic NACA0012 profile are shown, where the profile is excited either by a single quadrupole source or by a simplified deterministic turbulence volume. The results over the elastic profile are compared to those over a rigid one and are satisfying. The use of numerical tailored Green's functions will be considered in further investigations with more complex turbulence models.

ACKNOWLEDGEMENTS

The authors would like to thank Naval Group and *Association Nationale de la Recherche et de la Technologie* (ANRT) for supporting this work.

REFERENCES

1. MS Howe. Structural and acoustic noise produced by turbulent flow over an elastic trailing edge. *Proceedings of the Royal Society of London. Series A: Mathematical and Physical Sciences*, 442(1916):533–554, 1993.
2. William Devenport, Nathan Alexander, Stewart Glegg, and Meng Wang. The sound of flow over rigid walls. *Annual Review of Fluid Mechanics*, 50:435–458, 2018.
3. MS Howe. The turbulent boundary-layer rough-wall pressure spectrum at acoustic and subconvective wavenumbers. *Proceedings of the Royal Society of London. A. Mathematical and Physical Sciences*, 415(1848):141–161, 1988.
4. Stéphanie Chaillat, Benjamin Cotté, Jean-François Mercier, Gilles Serre, and Nicolas Trafny. Efficient evaluation of three-dimensional helmholtz green's functions tailored to arbitrary rigid geometries for flow noise simulations. *Journal of Computational Physics*, 452:110915, 2022.
5. Mathieu Aucejo. *Vibro-acoustique des structures immergées sous écoulement turbulent*. PhD thesis, INSA de Lyon, 2010.
6. Christophe Bogey, Christophe Bailly, and Daniel Juvé. Computation of flow noise using source terms in linearized euler's equations. *AIAA journal*, 40(2):235–243, 2002.
7. Daniel R Wilkes and Alec J Duncan. Acoustic coupled fluid–structure interactions using a unified fast multipole boundary element method. *The Journal of the Acoustical Society of America*, 137(4):2158–2167, 2015.
8. K Yoshida. *Applications of Fast Multipole Method to boundary integral element method*. PhD thesis, Department of Global Environment Engineering, Kyoto University, 2001.

9. Partha Pratim Goswami. *Application of the boundary element method to coupled fluid-structure interaction problems*. Iowa State University, 1991.
10. Huw G Davies. The radiated fields of multipole point sources near a solid spherical surface. *Journal of Fluid Mechanics*, 43(3):597–606, 1970.
11. James J Faran Jr. Sound scattering by solid cylinders and spheres. *The Journal of the acoustical society of America*, 23(4):405–418, 1951.
12. Michael James Lighthill. On sound generated aerodynamically i. general theory. *Proceedings of the Royal Society of London. Series A. Mathematical and Physical Sciences*, 211(1107):564–587, 1952.
13. DG Crighton and FG Leppington. On the scattering of aerodynamic noise. *Journal of Fluid Mechanics*, 46(3):577–597, 1971.
14. JE Ffowcs Williams and LH Hall. Aerodynamic sound generation by turbulent flow in the vicinity of a scattering half plane. *Journal of fluid mechanics*, 40(4):657–670, 1970.
15. WK Blake. Excitation of plates and hydrofoils by trailing edge flows. 1984.
16. GM Corcos and FS Sherman. The mixing layer: deterministic models of a turbulent flow. part 1. introduction and the two-dimensional flow. *Journal of Fluid Mechanics*, 139:29–65, 1984.
17. Neal P Sullivan, Shankar Mahalingam, and Robert M Kerr. Deterministic forcing of homogeneous, isotropic turbulence. *Physics of Fluids*, 6(4):1612–1614, 1994.